Food Hydrocolloids 133 (2022) 107959

Contents lists available at ScienceDirect

Food Hydrocolloids

journal homepage: www.elsevier.com/locate/foodhyd

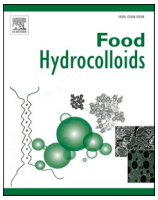

Promoted strain-hardening and crystallinity of a soy protein-konjac glucomannan complex gel by konjac glucomannan

Xinli Ran [a], Hongshun Yang [a,b,*]

[a] Department of Food Science & Technology, National University of Singapore, Singapore, 117542, Singapore
[b] National University of Singapore (Suzhou) Research Institute, 377 Lin Quan Street, Suzhou Industrial Park, Suzhou, Jiangsu, 215123, PR China

ARTICLE INFO

Keywords:
Molecular interaction
Konjac glucomannan
Soy protein
Aggregation
Crystallinity
Rheological performance

ABSTRACT

Protein-polysaccharide composite plays a substantial part in manufacturing plant-based meat and seafood alternatives. This research examined the impact of konjac glucomannan (KGM) concentrations on the molecular interactivities, gelation behaviors, and viscoelastic properties of a soy protein – konjac glucomannan complex gel, which was used as a model system for a plant-based fishball analog. The results revealed that increasing KGM concentration promoted the strain-hardening phenomenon of the complex gel, indicating an enhanced excluded volume interaction and the existence of large junction zones within the gel network. Additionally, increasing KGM level could extend the protein denaturation, exposing more buried functional groups, facilitating subsequent protein aggregation. Furthermore, as KGM rose from 0 to 8.0%, the gel strength S_g of the complex gel improved remarkably from 82.5 to 5537.6 Pa•s^n; contrastingly, the relaxation exponent n declined significantly from 0.72 to 0.12, revealing that KGM could facilitate the transition from sol to a more closely pure elastic solid. Interestingly, with the increased KGM incorporation, the relative crystalline index of the complex gel augmented from 26.79% to 53.08%, encouraging the construction of a regulated and compact gel network. Microstructure observations further supported that KGM induced a close-packed complex gel network with profound aggregations and large junctions. This study contributed to the further understanding of molecular interactivities between protein and KGM, providing fundamental support for the potential application of the KGM-protein complex in plant-based seafood alternatives.

1. Introduction

Proteins and polysaccharides are indispensable food ingredients that have been extensively utilized as structuring agents in the manufacturing of plant-based meat and seafood alternatives (Dekkers, Boom, & van der Goot, 2018). Gelation in food system containing protein or polysaccharide is critical for obtaining desired texture and sensory (Totosaus, Montejano, Salazar, & Guerrero, 2002). Protein gelation involves unfolding/denaturation of original protein structures, followed by the aggregation of the denatured structures, contributing to the formation of a three-dimensional gel network (Totosaus et al., 2002). Protein denaturation exposes functional groups (such as sulfhydryl groups, hydrophobic groups, etc.), generally enhancing the accessibility of potential interaction sites and facilitating the following aggregation (Berghout, Boom, & Van der Goot, 2015). The presence of polysaccharides could affect the intermolecular and intramolecular interactions within the complex system, possibly influencing the protein gelation behavior (Wang, Virgilio, Wood-Adams, & Heuzey, 2018). The molecular interactivities between these two ingredients plays a profound part in obtaining a certain texture and functionality of meat and seafood alternatives. Understanding the fundamental mechanism behind these interactions and their influence on overall product quality is critical for food processing involving both proteins and polysaccharides. Although the protein-polysaccharide mixed gel and their interactions have been extensively studied, many of these studies worked on the protein/κ-carrageenan mixed gel (Cao et al., 2021; Huang, Mao, Li, & Yang, 2021; Jiang, Ma, Wang, Wang, & Zeng, 2022); protein/xanthan mixed gel (Geremias-Andrade, Souki, Moraes, & Pinho, 2017; Zhang et al., 2019); protein/guar gum (Galante, Boeris, Álvarez, & Risso, 2017; Lei, Zhao, Li, Wang, & Wang, 2022). Konjac glucomannan (KGM), a polysaccharide extracted from *Amorphophallus* konjac roots, has been widely used in food processing. Little research was conducted concerning the KGM-protein mixed gel system and the effect of KGM on the functionalities of a specific food product. Despite a few studies

* Corresponding author. Department of Food Science & Technology, National University of Singapore, Singapore, 117542, Singapore.
E-mail address: fstynghs@nus.edu.sg (H. Yang).

https://doi.org/10.1016/j.foodhyd.2022.107959
Received 1 April 2022; Received in revised form 4 July 2022; Accepted 6 July 2022
Available online 14 July 2022

conducted, these studies focused on the effect of KGM on the gel qualities of low-value surimi (Iglesias-Otero, Borderías, & Tovar, 2010; Zhang, Li, Wang, Xue, & Xue, 2016), low-fat cheese (Dai, Jiang, Corke, & Shah, 2018), and low-protein noodles (Zhou et al., 2013), which included a hybrid system containing other ingredients such as starch and salt, making it difficult to specify the interactions involving KGM and the interactions among various compositions. Using model systems where the constituent compositions can be controlled and where the interactions between macromolecules can be evaluated may help better understand these interactions and establish the relationship between observed effects and the functionalities of a particular food product (Bernal, Smajda, Smith, & Stanley, 1987).

In the previous study (Ran, Lou, Zheng, Gu, & Yang, 2022), we incorporated soy protein isolate (SPI) with KGM, having developed a plant-based fishball analog imitating the texture of conventional fishball. Soy proteins are among the most common plant proteins utilized to produce plant-based meat products and seafood alternatives because of their availability, low cost, and comparable nutrition (Sha & Xiong, 2020). While SPI exhibits an overall good gelling performance, it is not advantageous to mock the texture of traditional seafood and red meat counterparts because the molecular association and structural alignment could not impart a meat-like fibrous structure (Sha & Xiong, 2020). KGM was used as a structuring agent to improve the textural and physicochemical properties of the plant-based fishball analogs in our prior study because of its impressive gelling capacity and water-holding capacity (Ran, Lou, et al., 2022). The prior study focused on the effect of KGM on macroscopic characteristics such as texture profile (hardness, chewiness, etc.) and product qualities at a macroscopic level. It was found that KGM significantly promoted the texture and rheological properties of the plant-based fishball analogs, in which the KGM was a major contributor to forming a specific texture similar to fishball. However, further study is necessary to comprehend the mechanism for the KGM impact on the plant-based fishball analogs at a microscopic level in a simplified model system.

To our knowledge, little research was performed using a model system to explore the molecular interactions between KGM and soy protein and the relationship of KGM-protein interactions with the functionalities (such as gelation) of the model system in plant-based seafood analogs. Therefore, through an SPI-KGM model system, this study aimed to elucidate the influence of KGM on the molecular interactivities, protein gelation, rheological behavior, and mechanical properties at the microscopic level; and to comprehend the relationship of these changes induced by KGM with the macroscopic functionalities of plant-based seafood analogs. The model system's dynamic mechanical thermal behavior, mechanical properties, relative crystalline index, molecular interaction forces, and microstructure were determined. These results demonstrated that the KGM could promote molecular interactivities, protein aggregation, crystallinity, and strain-hardening of the SPI-KGM model system for the plant-based fishball analogs, improving rheological behavior and mechanical property. This study could further provide a theoretical foundation for food manufactures to apply the KGM-protein complex in more varieties of plant-based seafood alternatives.

2. Materials and methods

2.1. Materials

Konjac glucomannan (KGM) and soy protein isolate powder (SPI) were acquired from iHerb Corporate (Moreno Valley, United States) and Myprotein (a sports nutrition brand, headquartered in Northwich, United Kingdom), respectively. Edible alkali (ingredient: sodium carbonate Na_2CO_3) was bought in a local supermarket in Singapore. All chemicals, including sodium chloride, bovine serum albumin (BSA), Biuret reagent, urea, 2-mercaptoethanol, Nile blue A, rhodamine B, and calcofluor white, are analytical grade and are purchased from Sigma-Aldrich Pte Ltd in Singapore.

2.2. Sample preparation

In our prior work, we have developed plant-based fishball analogs resembling the texture of traditional fishballs via incorporating SPI with KGM at different concentrations (3.5–8.0%) (Ran, Lou, et al., 2022). To further comprehend the KGM impact mechanism on SPI and the entire gel system, we prepared the SPI-KGM complex as a model system for the plant-based fishball analogs, with a fixed SPI level (10%, w/v) while different KGM levels (0–8.0%, w/v). The solution of Na_2CO_3 (0.5%, w/v) was used as a solvent for this model system and made up the weight difference. The unheated mixtures were directly used for rheological tests. Each mixture's deacetylation degree (DD) was also examined (Hu et al., 2019). As a result, the DD value for each mixture was 0%, 20.4%, 35.1%, 59.3%, and 74.4% (mass percentages), respectively. The mixtures were placed in sealed tin-foil dishes (with a diameter of 15.2 cm) and then steamed (90 °C, 30 min) in a water bath. These heated samples were placed inside a fridge at 4 °C for the following analyses. Samples prepared at three different times (three batches) were analyzed.

2.3. Rheological properties

2.3.1. Amplitude sweep test

Samples were under an amplitude sweep examination at 25 ± 0.01 °C using a rheometer configured with MCR 102 series and stress-controlled and (Anton Parr, Graz, Austria), with a strain from 0.01 to 100% and a steady frequency of 10 rad/s (Huang, Mao, Mao, & Yang, 2022). The distance between the sample stage and the parallel plate (diameter of 25 mm) was settled at 1.0 mm. The test was done to comprehend the linear viscoelastic region (LVR).

2.3.2. Dynamic mechanical thermal analysis (DMTA)

The oscillatory tests were done to interpret the dynamic mechanical thermal behavior described by Zhao, Chen, Hemar, and Cui (2020). The paste of the SPI-KGM complex was equilibrated (25 °C, 5 min) on the sample plate of the rheometer. Subsequently, a temperature sweep was executed with 0.5% of strain and 10 rad/s of angular frequency for three stages, including the heating stage (25–90 °C, 5 °C/min), equilibrium stage (90 °C, 10 min), and then cooling stage (90 - 25 °C, 5 °C/min).

2.3.3. Determination of mechanical spectra

A frequency sweep from 100 to 1 rad/s was executed at 0.5% of constant strain at different temperatures to examine gelling points (Yang, Yang, & Yang, 2018). The paste of the SPI-KGM complex was under heating (25–90 °C, 5 °C/min) to obtain initial gels and then measured under various balanced temperatures (35, 40, 45, 50, 55, 60, 65, 70, 75, and 80 °C, respectively). Variations in moduli G' and G'' versus angular frequency at various temperatures were recorded and analyzed.

2.4. Measurement for molecular interaction forces

The measurement for molecular interaction forces was conducted reached from the description of Zhang et al. (2016), where these forces were indirectly determined by measuring the protein solubility of samples under various chemical agents. These agents can cleave molecular bonds, including electrostatic and hydrogen bonding (sodium chloride solution with 0.6 mol/L), hydrogen bonding (urea solution with 1.5 mol/L), hydrophobic interactions and hydrogen bonds (urea solution with 8 mol/L), and S–S bonds (2-mercaptoethanol with 0.5 mol/L) (Zhang et al., 2016). Therefore, samples were treated by the following cleavage agents: (1) solution A, sodium chloride solution (0.05 mol/L); (2) solution B, sodium chloride solution (0.6 mol/L); (3) solution C, sodium chloride solution (0.6 mol/L) + urea solution (1.5 mol/L); (4) solution D, sodium chloride solution (0.6 mol/L) + urea solution (8.0

mol/L); (5) solution E, 2-mercaptoethanol (0.5 mol/L) + sodium chloride solution (0.6 mol/L) + urea (8.0 mol/L). Proteins would be partly solubilized in these chemical agents. The ionic bonding (expressed as protein solubility variance between solution B and A), hydrogen bonding (expressed as protein solubility variance between solution C and B), hydrophobic interactions (expressed as protein solubility variance between solution D and C), and disulfide bonding (expressed as protein solubility variance between solution E and D) were determined. Chopped samples (2 ± 0.02 g) were treated with each chemical solution in a handheld homogenizer (D-130 model, Wiggens Co., Ltd, Beijing, China) at 8000 rpm for 2 min. The homogenates were oscillated at 4 °C for 60 min, followed by centrifugation (Sartorius Centrisart® D-16C, 5 min, 8000×*g*). The concentration of solubilized protein was evaluated via the Biuret experiment (Han et al., 2021). The measurement was performed based on the description by Niu et al. (2013). Bovine serum albumin (BSA) was utilized as a protein standard. A mixture of BSA, 0.85% NaCl, and Biuret reagent was measured using a UV–Vis spectrometer (Shimadzu UV-1280, Shimadzu Corporation, Singapore) at 540 nm to obtain a standard curve (protein concentration vs. absorbance). A mixture of the sample and Biuret reagent was then stood for 30 min at room temperature and was examined under the same UV–Vis spectrometer to acquire the absorbance of the mixture. The protein solubility of each sample is the ratio of solubilized protein to homogenate (mg/mL).

2.5. Powder X-ray diffraction (XRD)

Powder XRD is a technique to assess materials' crystallized structures (Liang, Liao, Qi, Jiang, & Yang, 2022). The test was executed via a Powder X-ray Diffractometer (*Bruker D8 Advance*, Germany). Freeze-dried gels were measured at a 2θ ranging from 4° to 60°, with 0.2° of step size and 2°/min of scan rate. The resulting spectra were integrated using the peak analyzer tool of Origin 2021b software (OriginLab Corporation, Northampton, United States). The relative crystallinity index (CI, %) were expressed as follows (Kumar, Brennan, Brennan, & Zheng, 2022):

$$CI(\%) = \frac{A_c}{A_c + A_a} \times 100 \quad (1)$$

A_c represents the area for crystalline portion, A_a represents the area for amorphous portion, and $A_c + A_a$ represents the overall area for the XRD diffractogram.

2.6. Fourier transform infrared spectroscopy (FTIR)

A Fourier transform infrared spectrophotometer (PerkinElmer, USA) was utilized for obtaining the gels' FTIR spectra. The freeze-dried gels and KBr (1: 50 mass ratio) were ground together to prepare for tablets for further measurements (Sow, Toh, Wong, & Yang, 2019). The prepared sample tablets were put in a specimen chamber and scanned at 4 cm^{-1} of resolution and 32 scans (4000–450 cm^{-1}) (Sow, Nicole Chong, Liao, & Yang, 2018). The resulting FTIR spectra were processed and analyzed with the Origin 2021b software.

2.7. Confocal laser scanning microscopy (CLSM)

The Zeiss *LSM 710* Confocal Microscope (Carl Zeiss AG, Jena, Germany) was utilized to visualize samples' microstructures. Rhodamine B (0.1%, w/v) prepared in isopropanol and Calcofluor white stain were used for staining proteins and polysaccharides (Feng, Wang, Wang, Xia, & Huang, 2021), respectively. Gels sliced into thin pieces (2 ± 0.5 mm in thickness) were immersed in a combined stain (1.0 mL Rhodamine B + 1 drop of Calcofluor white) for 1 min and then washed with DI water three times. The stained samples were stored overnight for CLSM analysis. The samples were observed under a 10× objective lens and tracked at channel 1-Calcofluor white and channel 2-Rhodamine B. The excitation wavelength for channels 1 and 2 was 405 and 488 nm, respectively.

2.8. Statistical analysis

Experimental tests were independently conducted in triplicates, and these results were processed in SPSS 20.0 (IBM Corp., Armonk, NY, USA). The statistical difference among different groups was assessed via one-way variance analysis (ANOVA). The statistically significant variations were determined once the *P*-value < 0.05.

3. Results and discussions

3.1. Amplitude sweep analysis

The typical relationship between viscoelastic modulus and shear strain γ is shown in Fig. 1A, including (I) the linear viscous region, (II) the nonlinear viscoelastic region (NLVR), and (III) the viscoelastic region (LVR). The LVR and NLVR will be discussed in this study to investigate the viscoelastic characteristics of those SPI-KGM gel mixtures. A critical strain (γ_{cr}) is identified as the limit for LVR (G′ deviates within 5%), and a further increase of strain ($\gamma > \gamma_{cr}$) results in nonlinear viscoelastic behavior (G′ differs more than its 5%) (Abbastabar, Azizi, Adnani, & Abbasi, 2015).

Within the LVR ($\gamma < \gamma_{cr}$), G′ and G″ scarcely varied with amplitude strain (Fig. 1A), revealing that the gel networks are strong enough to obstruct the structure breakdown caused by the oscillatory shearing (Chemeda, Deneele, Christidis, & Ouvrard, 2015). In other words, the γ_{cr} is an indicator of shape retention and structure strength under exterior stress (Hesarinejad, Koocheki, & Razavi, 2014). As shown in Table 1, with the elevating KGM concentration, γ_{cr} increased significantly from 0.68% to 2.20%, indicating an increased structure strength by KGM. Notably, both G′ and G″ of gels with higher KGM levels were considerably enhanced (Fig. 1B), which further confirmed that the presence of KGM impressively improved the structural strength of the compound SPI-KGM gel. These phenomena could be because increasing KGM levels promoted the deacetylation degree (DD) of the SPI-KGM mixtures (the measurement of deacetylation degree showed that the DD of each mixture was 0%, 20.4%, 35.1%, 59.3%, and 74.4%, respectively). The removal of acetyl groups through deacetylation could increase the hydrophobicity of KGM molecules (Chen, Li, & Li, 2011). Meantime, during deacetylation under alkaline condition, the acetyl groups on KGM molecules could be replaced with hydroxyl groups, facilitating the formation of hydrogen boding interactions (Li, Ma, Chen, He, & Huang, 2018). Consequently, increasing KGM concentration in the mixtures could improve the hydrogen bonding and hydrophobic interactions (Zhang, Xue, Li, Wang, & Xue, 2015) within KGM molecules and between KGM and SPI molecules. Prior research has indicated that more interchain interactions among KGM molecules contributed to forming more flexible and denser gel network (Solo-de-Zaldívar, Tovar, Borderías, & Herranz, 2014). Moreover, KGM has been demonstrated to have an excellent water absorption capacity due to its numerous hydroxyl groups, leading the free water to transform into bound water (Xiong et al., 2009). Water in the SPI-KGM gel matrix can be considered as a plasticizing agent that would impart the gel moldable and less brittle, leading to a higher γ_{cr}.

With further increasing strain ($\gamma > \gamma_{cr}$), the storage modulus G′ gradually reduced, indicating a breakdown of inter-particle network structures. At the same time, G″ presented an interesting strain-hardening phenomenon distinguished by a bulge at strain amplitude γ_{max} with a maximum G''_{max} (Fig. 1A and Table 1). This strain-hardening phenomenon occurs due to excluded volume interaction that would restrict shear-induced particle motion (Chemeda et al., 2015). Previous research conducted by Bossard, Moan, and Aubry (2007) has suggested that the excluded volume interaction is influenced by electrostatic repulsive interaction and inter-particle distance fluctuation, playing a significant part in materials' viscosity and elasticity.

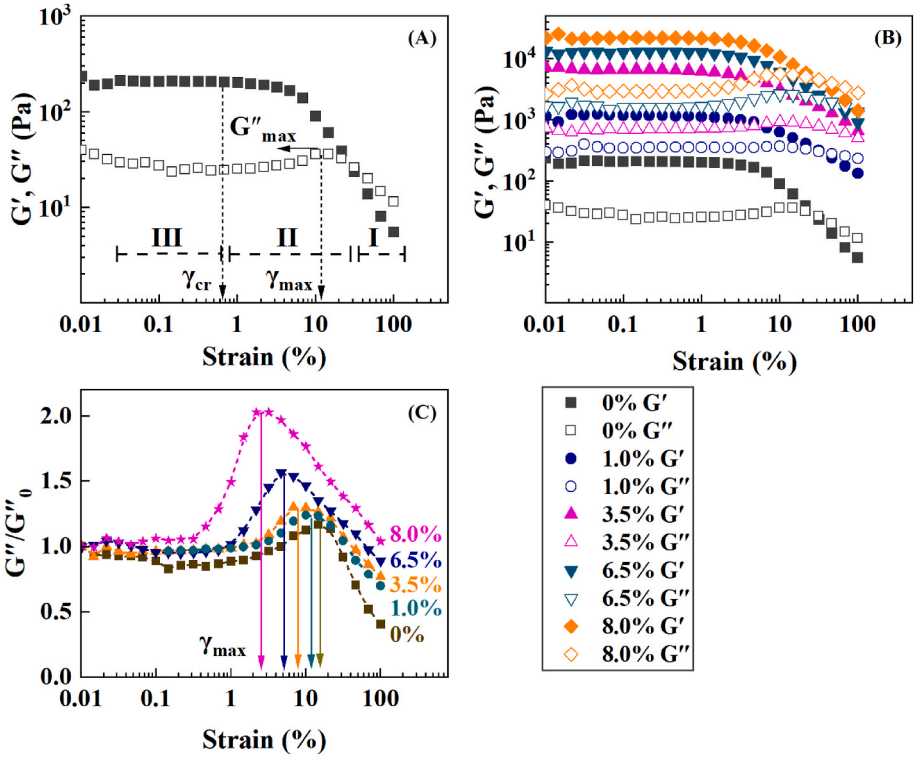

Fig. 1. (A) The typical plots for storage modulus G′ and loss modulus G″ against shear strain. (B) Amplitude sweeps spectra for the complex at different konjac glucomannan (KGM) concentrations. (C) The plot for declined loss modulus G″/G″0 of samples against shear strain.

Table 1
Parameters from amplitude sweep for the SPI-KGM complex with different KGM concentrations.

	γ_{cr} (%)	G''_{max} (Pa)	γ_{max} (%)	Peak of G''/G''_0
0%	0.68 ± 0.05^{d}	35.8 ± 3.2^{e}	14.80 ± 0.58^{a}	1.16 ± 0.05^{d}
1.0%	1.01 ± 0.08^{c}	366.1 ± 54.3^{d}	10.11 ± 0.62^{b}	1.24 ± 0.09^{c}
3.5%	1.01 ± 0.10^{c}	910.7 ± 69.2^{c}	6.92 ± 0.28^{c}	1.29 ± 0.12^{c}
6.5%	1.48 ± 0.03^{b}	2615.5 ± 87.3^{b}	4.72 ± 0.31^{d}	1.56 ± 0.18^{b}
8.0%	2.20 ± 0.11^{a}	5636.8 ± 89.5^{a}	2.21 ± 0.24^{e}	2.03 ± 0.17^{a}

Note: (1) SPI, soy protein isolate; KGM, konjac glucomannan. (2) The different alphabets for each parameter represent a statistically significant difference ($P < 0.05$).

As shown in Fig. 1C, the relative change of the loss modulus G" (regardless of the physical meaning) of SPI-KGM complex with different KGM concentration (0–8.0%) were considered, which would provide further information about the density of gel networks (porous or packed structures). The intensity of strain hardening (the peak of $G"/G"_0$ curves) and γ_{max} (the strain values at $G"_{max}$) of SPI-KGM gels impressively varied with KGM levels. With the KGM concentration elevated from 0 to 8.0%, the extent of strain-hardening of gels increased significantly from 1.16 to 2.03. Besides, with elevating KGM addition, the strain hump became wider (also lower γ_{max}) for the complex gels (Fig. 1C). These observations revealed that in the presence of higher KGM concentration, the molecular motion in the SPI-KGM complex resulting from oscillatory shearing was more restricted, leading to less inter-particle distance fluctuation. Prior studies have noted that the protein gelation induced by heating consists of complicated processes, including unfolding/denaturation, dissociation-association, and the further aggregation of denatured protein molecules (Hermansson, 1986; Speroni et al., 2009). During heating, the protein denaturation would expose the hidden hydrophobic residues and present high negative electrostatic repulsion (Hogan, Daly, & McCarthy, 2021). It could be because KGM may promote the protein denaturation (further discussed in the following DMTA analysis), increasing electrostatic repulsive interaction in the SPI-KGM complex. Bossard et al. (2007) have demonstrated that increasing electrostatic repulsive interaction may decrease inter-particle distance throughout oscillatory shear measurement; the decreased inter-particle distance could enhance electro-viscous dissipation and steric interaction, strengthening excluded volume interaction and thereby promoting the strain-hardening phenomenon (the hump of the G″ curve). Furthermore, Baeza, Carp, Pérez, and Pilosof (2002) have demonstrated that increasing excluded volume effects in the protein-polysaccharide (κ-carrageenan) system would facilitate the constitution of robust junction zones within the three-dimensional networks, favoring the gelation of the compound gel system. Similarly, deacetylation of KGM could eliminate the acetyl groups on the KGM molecules, forming deacetylated KGM that helps build junction zones via hydrogen bonds (Herranz, Tovar, Solo-de-Zaldívar, & Borderias, 2012). KGM at a higher concentration (up to 8.0%) had a more substantial deacetylation degree (up to 74.4%), enhancing the size and number of these junction zones, which could affect the thermal and rheological behaviors of the formed gels (Solo-de-Zaldívar et al., 2014).

3.2. Dynamic mechanical thermal analysis (DMTA)

Variations in rheological performance during thermal treatments could be related to structural changes such as the association of KGM chains, and the unfolding and aggregation of proteins (Huang, Theng, Yang, & Yang, 2021). Accordingly, the DMTA was implemented to understand the temperature impact on structural formation during thermal treatment. Fig. 2 and Fig. S1 display the relationship of moduli (G′, G″) with temperature and time. The following discussion will predominantly focus on the changes in G′ (an indicator of stiffness) during thermal treatment (Fig. 2), for a similar trend was found in G″ (Fig. S1).

The complex without KGM addition showed a notably different trend during the heating process from other mixtures containing KGM (Fig. 2). Specifically, as temperature increased, the moduli of the mixture without KGM decreased progressively first, followed by a rapid increase

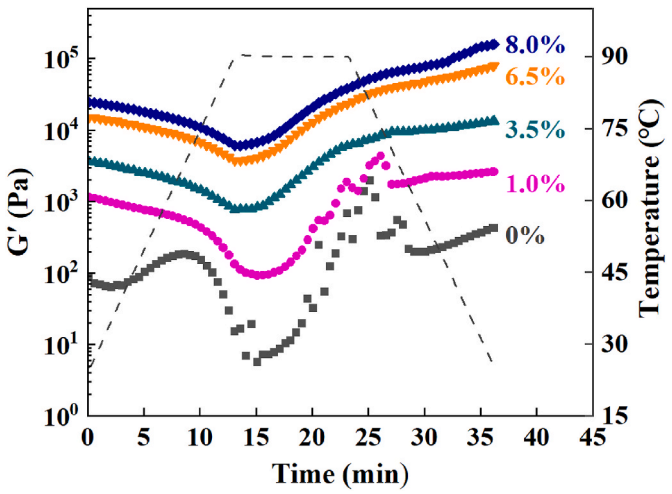

Fig. 2. The changes of storage modulus G′ of samples against time during temperature sweep (heating, holding, and cooling procedures).

at around 40 °C until 68 °C. Lastly, a swift drop of G′ was found until the end of the heating procedure. This phenomenon could be explained by the heat-induced gelling process of soy protein, primarily including unfolding/denaturation (G′ decreases), followed by aggregation and rearrangement (G′ increases) (Renkema & van Vliet, 2002). Two possible mechanisms were involved regarding the second G′ decrease around 68 °C. The high temperature (>68 °C) could destroy the hydrogen bonding connecting crosslinks, interrupting the formed three-dimensional network (Luo, He, & Lin, 2013). Previous studies have shown that the denaturation of soy protein conglycinin and glycinin is related to the G′ peaks at around 68 °C and 80 °C during heating (Comfort & Howell, 2002; Renkema & van Vliet, 2002; Wu, Hua, Chen, Kong, & Zhang, 2017). Additionally, crystalline structure, where the molecules are held together in an ordered three-dimensional arrangement, is linked to the rheological characteristics of materials (Rønholt, Kirkensgaard, Pedersen, Mortensen, & Knudsen, 2012). Champenois, Rao, and Walker (1998) have indicated that the melting of crystalline structure could lead to the decrease in stiffness (reduced G′). Therefore, it is probably that the crystal structure melts at 68.1 ± 0.2 °C, resulting in the second decrease of G′ (Huang, Theng, et al., 2021). The melting temperature of crystal structure could be heightened with KGM addition (melting at 68.1 ± 0.2 °C, 70.0 ± 0.5 °C, 73.1 ± 0.2 °C, 75.6 ± 0.4 °C, and 76.6 ± 0.1 °C for the system with 0%, 1.0%, 3.5%, 6.5%, and 8.0%, respectively), possibly because KGM could protect crystal structures during heating (decreased heat transfer) (Zhou et al., 2014).

Interestingly, with the increase of KGM concentrations, the G′ was increased impressively (Fig. 2). Renkema et al. (2002) reported the correlation between the G′ of soy protein gels and the protein denaturation during heating, indicating that a higher G′ value could be related to a higher degree of protein denaturation. Therefore, the increased G′ values in the system with higher KGM concentration could be because KGM promoted the soy protein denaturation during heating. Besides, the duration of the initial decrease of the G′ was extended progressively until the terminal of the heating procedure (Fig. 2), implying a longer denaturation process in the mixtures with higher KGM concentrations. Similar curves during temperature sweep were also observed during SPI (17% w/w) gelation in a previous study (Comfort et al., 2002), where they ascribed the initial decrease of G′ to the denaturation of globulins. Fundamentally, the denaturation of protein structures could make the functional groups (such as hydrophobic groups) exposed, facilitating the followed aggregation procedure and the formation of three-dimensional networks (gel networks) (Matos, Sanz, & Rosell, 2014). A possible explanation for the extended denaturation may be that KGM would prevent the inner temperature of samples from immediately elevating as KGM formed a highly dense matrix under alkaline conditions, decreasing heat transfer efficiency (He et al., 2020). Consequently, the temperature was not enough for the subsequent aggregation and rearrangement immediately. Renkema et al. (2002) have suggested that a certain number of denatured proteins is needed for gelling process as the unfolded and denatured protein structures expose hydrophobic and sulfhydryl groups, which would interact with each other, forming irrevocable protein aggregation and strengthening gel networks. Therefore, the gelling process was prolonged, and the temperature for gelling was escalated. Moreover, Baeza et al. (2002) indicated that denatured protein structures could expose hidden functional groups and reinforce electrostatic repulsive forces, facilitating excluded volume effect, which could increase the electrostatic interactions between the protein and KGM and among protein molecules (Baeza et al., 2002), therefore improving the stiffness of final gels (enhanced G′). These observations further supported the earlier discussion that KGM could facilitate excluded volume interaction and promote the strain-hardening phenomenon. Unexpectedly, the gelling (sol to gel) temperature for SPI-KGM samples with 1.0%, 3.5%, 6.5%, and 8.0% was not observable on the DMTA curves, that is, no crossover points of G″ and G′ (Yang et al., 2018) or no sharp increase in G′ during cooling (Zhao et al., 2020), possibly due to the rapid heating and cooling rate (5 °C/min). It has been demonstrated that the heating and cooling rate would influence the gelling behavior (Yang et al., 2018); therefore, we applied the Winter-Chambon and scaling laws in the subsequent analysis (section 3.3) to acquire the gelling temperature regardless of the heating rate.

During the temperature holding procedure (90 °C, 10 min), the moduli for all samples showed an upward trend (Fig. 2), indicating the formation of strengthened structures. Prior research by Liu and Hsieh (2007) has denoted that the initial heating of soy protein could generate a reversible pre-gel that would be interrupted upon further heating and transformed into an irreversible gel with structures linked by covalent bonding (disulfide). Accordingly, the generation of gel structures with covalent bonds would contribute to gel strength and firmness. Another indication from the dynamic thermal curves was that with KGM concentration increased from 1.0% to 8.0%, the onset where G′ started growing shifted toward the left progressively; meantime, the G′ remained higher for the complex gel with higher KGM addition, implying slower gelation occurred for the sample with higher KGM addition. Similarly, Chen et al. (2011) have suggested that the slower the gelation occurs, the greater the storage modulus G′ is. The slower gelation facilitates the incorporation of molecular chains to form three-dimensional elastic networks, favoring the formation of a uniform and elastic protein-polysaccharide gel (Zhuang, Wang, Jiang, Chen, & Zhou, 2021).

During the cooling procedure from 90 to 25 °C (Fig. 2), a maintained augment in G′ was observed for all samples, suggesting the reinforced covalent and non-covalent bonding among molecular chains through cooling, further improving the strength and stability of the formed gel networks. The hydrogen bonds and hydrophobic interaction would be enhanced at low temperatures; meanwhile, the electrostatic repulsion forces among protein side chains may be restrained (Zhao et al., 2020). Furthermore, the disulfide bonds among protein molecules would also be enhanced in the cooling process (Campbell, Gu, Dewar, & Euston, 2009). Hesarinejad et al. (2014) indicated that the cooling process increased the G′ value of a gel containing *Lepidium perfoliatum* seed gum, attributed to the strengthened hydrophobic interactions during cooling. Similarly, Rafe and Razavi (2013) concluded that the increasing G′ of basil seed gum during cooling occurred because cooling enhanced hydrogen bonding.

3.3. Mechanical properties

Evidence has shown that heating or cooling rate would influence gelling points (Liu, Bao, & Li, 2016); meanwhile, the applied frequencies would also influence the gelling temperatures (Sow, Tan, & Yang, 2019).

For these reasons, we utilized the Winter-Chambon and scaling law to determine a more accurate gelling temperature. Following the Winter-Chambon gel equation, the moduli (G′, G″) display a power-law correlation with the angular frequencies at gelling position (Yang et al., 2018).

$$G'(\omega) \sim G''(\omega) \sim \omega^{n} \tag{2}$$

Moreover, the stress relaxation modulus G (t) at the gelling position can be expressed as follows:

$$G(t) = S_g \cdot t^{-n} \tag{3}$$

The relaxation rate at the gelling position is expressed as the *n* value (relaxation exponent or power-law strength) in equation (3); the critical gel strength at the corresponding position is expressed as the S_g value ($Pa \cdot s^n$), which can be simply interpreted as the stress relaxation modulus value with a relaxation time t = 1 s at the gel point.

Furthermore, the loss factor (tan δ) of a material is expressed as follows:

$$\tan\delta = \frac{G''(\omega)}{G'(\omega)} = \tan\left(\frac{n\pi}{2}\right) \tag{4}$$

Consequently, the gelling temperature at the critical gelation position can be obtained when tan δ is not correlated to ω.

The changes in moduli (G′, G″) with ω at various temperatures governing gelling process is illuminated in Fig. S2. The data were shifted perpendicularly by 10^a to be prevented from overlapping. The G′ was proportional to $\omega^{0.05\text{-}0.22}$, while G″ was proportional to $\omega^{0.10\text{-}0.25}$. Besides, G′ predominated over G″ considerably during the entire angular frequencies, representing a classic viscoelastic solid performance. Furthermore, the variance between G′ and G″ became peculiarly remarkable at higher temperatures, signifying a specific gelling process.

To acquire the gelling temperatures for each sample, we plotted the curves for tan δ at various ω against temperature (Fig. 3). The critical gelling temperature of each sample was determined as the crossover of multifrequency curves (Sow, Tan, & Yang, 2019), suggesting the independence of tan δ with the frequency at the specific temperature (Yang

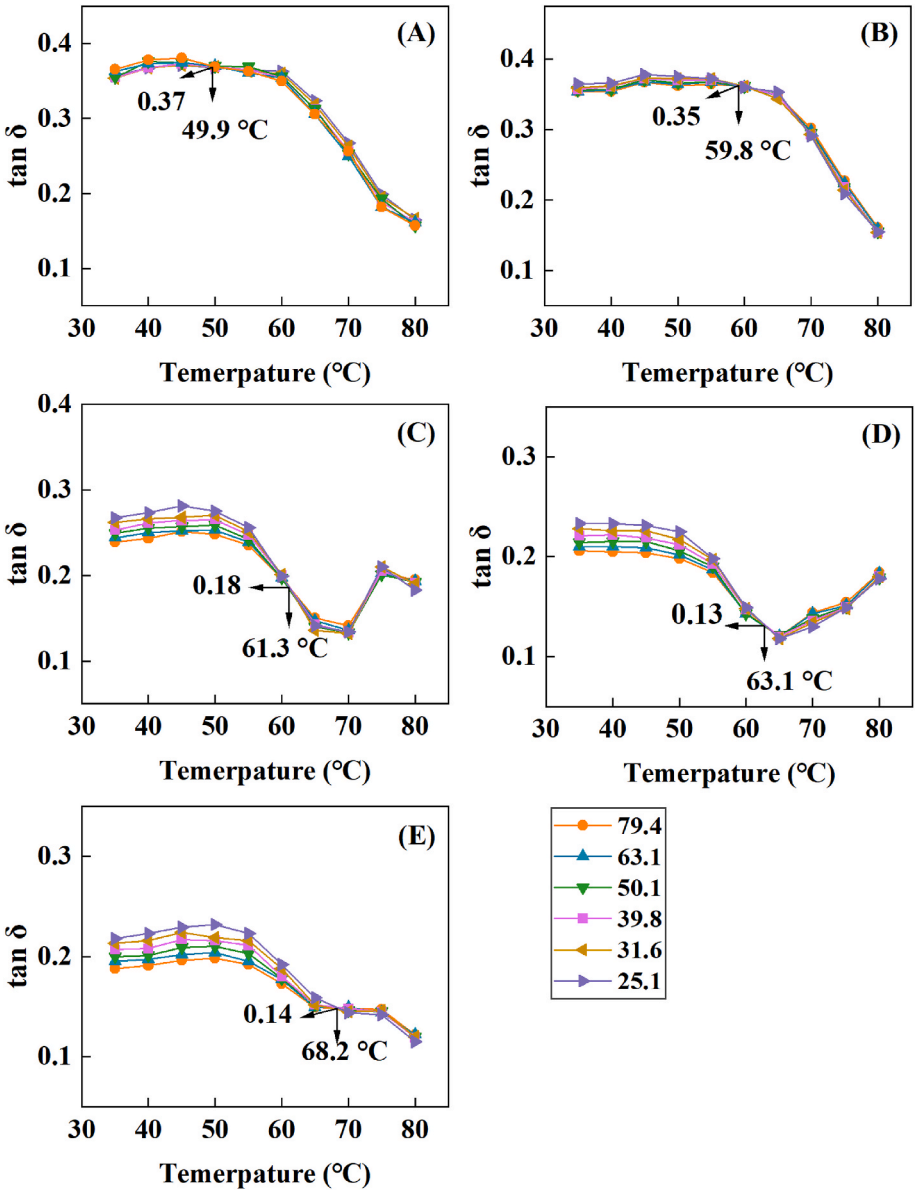

Fig. 3. The variation of loss factor tan δ with temperature at various angular frequencies. (A) The SPI-KGM complex containing 0% of konjac glucomannan (KGM), (B) the SPI-KGM complex containing 1.0% KGM, (C) the SPI-KGM complex containing 3.5% KGM, (D) the SPI-KGM complex containing 6.5% KGM, (E) the SPI-KGM complex containing 8.0% KGM.

et al., 2018). The crucial tan δ values and corresponded gelling temperatures are indicated in Fig. 3. Principally, tan δ < 1 signifies G′ is predominated versus G″; in contrast, tan δ > 1 signifies G″ is predominant versus G′ (Huang, Mao, et al., 2021). Therefore, all samples presented an elastic attribute predominantly (tan δ < 1). Raising KGM concentration resulted in an overall lower tan δ value, implying that KGM improved the elastic property of the SPI-KGM complex. Likewise, a previous study has disclosed that KGM could enhance the hardness and elasticity of a low-fat cheese product (da Silva, de Souza Ferreira, Bruschi, Britten, & Matumoto-Pintro, 2016). Corresponding to critical gel points, the gelling temperature for samples with KGM levels from 0 to 8.0% was 49.9 °C, 59.8 °C, 61.3 °C, 63.1 °C, 68.2 °C, respectively (Fig. 3), demonstrating that KGM increased the gelling temperature progressively, possibly because KGM protected the inner temperature of the complex from immediate elevating. This observation was in accordance with the earlier discussion that KGM could promote the SPI denaturation and aggregation.

In addition, the relaxation exponent n is associated with the junction zones density (the extent of gel connectivity). Herranz et al. (2012) have stated that a lower n value indicates a higher crosslink density, which enhances the degree of junction zones within the gel networks. The n value for sample 0%, 1.0%, 3.5%, 6.5%, and 8.0% was 0.72, 0.43, 0.23, 0.15, and 0.12 (Fig. 4). Generally, the material with $n = 0$ possesses a completely elastic performance, while the material with $n = 1$ possesses a wholly viscous performance (Yang et al., 2018). The SPI-KGM complex with 6.5% and 8.0% KGM had a significantly lower relaxation exponent n than other groups, revealing that KGM with high concentration could facilitate the sol-gel evolution more closely to a purely elastic solid. Therefore, a lower n value indicates a more significant gel network density and structural strength.

It is noteworthy that the power-law strength n was correlated with fractional dimension d_f, with which the relationship was described as follows (Huang et al., 2022):

$$n = \frac{d\,(d+2-2\,d_f)}{2\,(d+2-d_f)} \tag{5}$$

The d ($d = 3$) represents the space dimension, while d_f represents the fractal dimension. The resulting d_f values based on equation (5) are shown in Fig. 4, where the d_f increased from 1.71 to 2.39 pronouncedly as KGM concentration increased from 0 to 8.0%. This observation was consistent with prior research showing that the d_f value for a system containing polysaccharides ranged from 1.7 to 2.5 (Lu, Liu, & Tong, 2006). The fractal dimension d_f could illustrate the quality and quantity of aggregated structures (Andoyo, Dianti Lestari, Mardawati, & Nurhadi, 2018). It has been denoted that the d_f value above 2.0 suggests reaction-limited cluster-cluster aggregations; contrastively, the d_f value between 1.7 and 1.8 suggests diffusion-limited cluster-cluster aggregations (Andoyo et al., 2018). Substantially, a high d_f value signifies dense aggregated structures, while a low d_f value signifies loose aggregated structures (Andoyo et al., 2018). Therefore, the increment of the d_f demonstrated that KGM could enhance the density of aggregated structures, which could be attributed to the enhancement of large junction zones.

Another significant finding was that the gel strength S_g was improved remarkably from 82.5 to 5537.6 Pa•s^n with the increasing KGM levels (Fig. 4). The parameter S_g is associated with the size and the number of network junctions (Liu et al., 2016), implying the physical structure strength. Therefore, it could be inferred that increasing KGM concentration would promote the number and size of junction networks, resulting in a denser and strengthened gel.

3.4. X-ray diffraction analysis

The X-ray diffraction (XRD) examination measures the intra- and intermolecular interactions within polymer networks, determining crystalline (broad and diffuse peaks) or amorphous properties. The crystalline characteristics could be comprehended as ordered in the short-range and unordered in the long-range (Brindley, 1980). The XRD pattern of the SPI-KGM complex with different KGM concentrations is shown in Fig. 5A. All samples exhibited a typical amorphous-dominated curve with low peak intensity and crystallinity. These peaks were generally broad and weak, probably because specific protein crystalline structures were melted during the heat-induced gelling process.

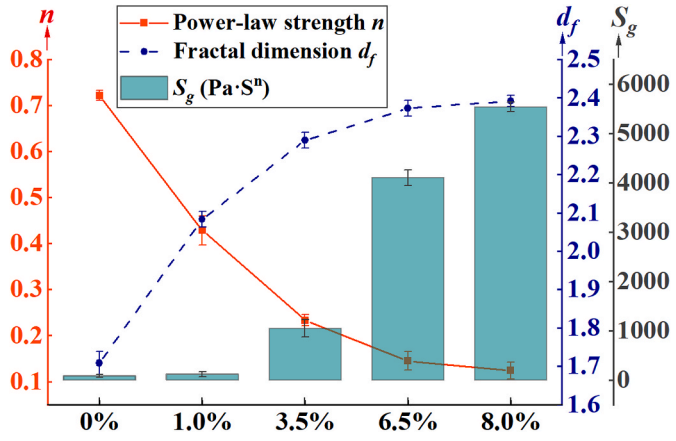

Fig. 4. The dependence of power-law strength n, fractional dimension d_f, and the gel strength S_g with konjac glucomannan concentration in SPI-KGM complex gels.

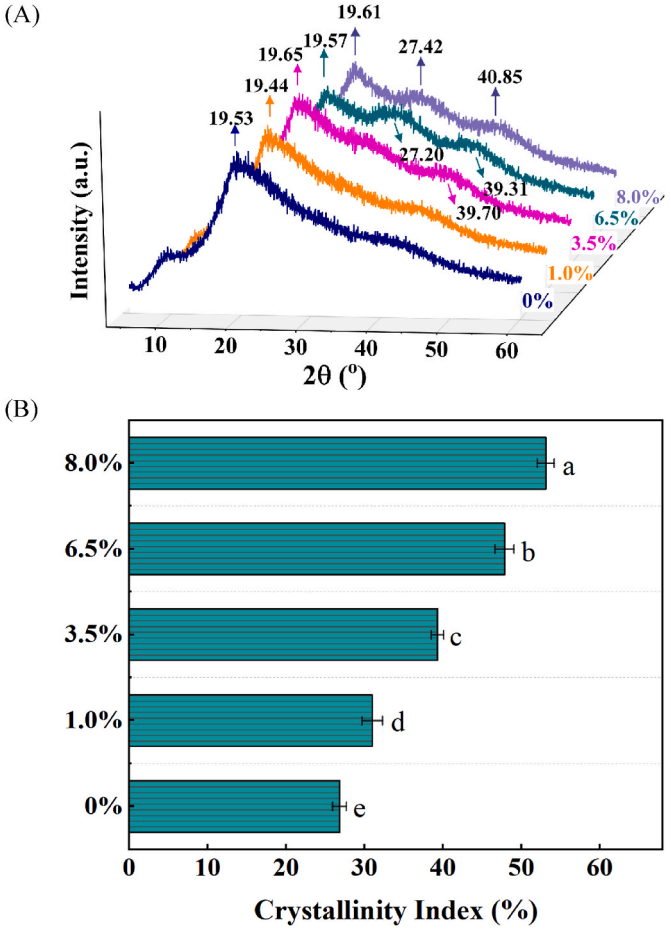

Fig. 5. (A) The Powder-XRD pattern and (B) the relative crystallinity index for SPI-KGM complex containing 0%, 1.0%, 3.5%, 6.5% and 8.0% of konjac glucomannan.

Furthermore, a noticeable difference in peak numbers was found between the sample without KGM and samples with KGM addition. Specifically, a broad peak around $2\theta = 19^{\circ}$ was observed for all samples, while one additional subtle peak around $2\theta = 40^{\circ}$ was observed for sample with 3.5% KGM; two additional subtle peaks around $2\theta = 27^{\circ}$ and 40° were observed for samples with 6.5% KGM and 8.0% KGM. These additional peaks of the SPI-KGM complex gel demonstrated that the interaction between SPI and KGM and the aggregation among polysaccharide chains contributed to regulated arrangements and regular structures, facilitating the long-range order and increasing crystallinity (Yuan, Xu, Cui, & Wang, 2019). Similarly, peaks were also found around $2\theta = 19^{\circ}$, 28°, 40° in a carrageenan-KGM complex system (C. Yuan, Xu, et al., 2019).

The relative crystallinity index (CI) was estimated for each sample. As shown in Fig. 5B, as KGM concentration increased from 0 to 8.0%, the CI value was progressively enhanced from 26.79% to 53.08%. Prior research has indicated that deacetylated and native KGM primarily exhibited an amorphous state (Zhang et al., 2016). KGM is a non-crystalline polysaccharide (Wang, Zhou, Wang, & Li, 2015) and an amorphous polymer (Tatirat & Charoenrein, 2011). Previous studies have reported the existence of crystalline structure from soybean 7S β-conglycinin and 11S globulin (Maruyama et al., 2001; Su, Huang, Yuan, Wang, & Li, 2010; Zhang, Xue, et al., 2015). It could be assumed that KGM with high concentration protected SPI crystalline structure from melting at high temperatures, reserving more crystalline structures in the SPI-KGM complex. Similarly, KGM was demonstrated to protect crystalline structure of canna starch and wheat starch from melting during heating (Liu et al., 2021; Zhou et al., 2014).

Furthermore, a higher crystalline index could signify a robust structural strength because the molecular interactivities are more considerable at a crystalline state (Balani, Verma, Agarwal, & Narayan, 2014). A higher crystallinity could also indicate a more significant density and stiffness of the gel networks (McKeen, 2012). These observations were consistent with the previous discussion that KGM could strengthen the gel strength of the SPI-KGM complex gel.

3.5. Microstructural observations

The resulting CLSM images with different KGM concentrations are depicted in Fig. 6A–E, where the rhodamine B-tracked channel was treated with grayscale to reduce color contrast. The polysaccharide KGM in the complex gel was labeled using Calcofluor white (blue portions) (Fig. 6B1-E1), allowing for the observation of the spatial arrangement and profile of KGM molecular chains. As KGM concentration increased, the Calcofluor white-stained KGM structure (in color blue) transformed from irregular filamentous to a packed and fibrous network matrix. Meantime, the protein microstructure of the SPI-KGM complex gel was also evidently changed with KGM concentration (Fig. 6A2-E2). Specifically, the protein structures in the gel network without KGM were relatively scattered and not well aggregated. Upon adding KGM to the complex, these scattered protein structures became arranged and aggregated; moreover, increasing KGM concentration in SPI-KGM complex gel promoted the extent of protein aggregations and clusters, helping form a well-constructed gel network.

The overlap images for channels 1 and 2 were marked as A3 to E3, corresponding to the sample with 0%, 1.0%, 3.5%, 6.5%, and 8.0% of KGM. The Calcofluor white-stained KGM was progressively dispersed throughout the SPI matrix with the elevating KGM concentration. All the complex gels containing KGM presented uniform fluorescence intensity, indicating the existence of protein-KGM interactions (possibly hydrogen bonds). It is possibly that the SPI molecules presumably interacted and occupied the void of the KGM network matrix, forming a filled and compact complex gel, of which the degree of packed structures increased with the increasing KGM concentration. Notably, an excessive KGM concentration ($\geq$ 8.0%) led to an overly compact gel network, which could result in a rigid texture of the complex gel.

These phenomena could be probably because that KGM extended the initial protein's denaturation, increasing functional groups, which could facilitate further aggregation. Besides, KGM could also promote the exposure of hydrophobic residues of protein chains by prolonging the denaturation procedure (Li, Wang, Zheng, & Guo, 2019), further improving protein aggregations. Consistently, KGM has also increased the aggregation of gluten proteins (Wang et al., 2017) and myofibrillar proteins (Yuan, Yu, et al., 2019) by enhancing hydrophobic interactions. Microstructural observations further supported the previous results that increasing KGM concentration would elevate the storage modulus G′ and gel strength.

3.6. A proposed schematic model

Reached from the observations mentioned above, we have put forward a schematic diagram to illustrate the possible mechanism of KGM impact on the SPI-KGM complex (Fig. 7). During heating, the compact oligomers 7S β-conglycinin and 11S glycinin were dissociated into monomers, exposing the functional groups, such as sulfhydryl, hydrophobic, and amine groups. The exposed functional groups could further promote the followed protein aggregation (Matos et al., 2014) and interactivities between the protein with KGM molecules, leading to the formation of three-dimensional networks (gel networks). Increasing KGM concentrations could extend the duration of the protein denaturation and slow down the gelling procedure (higher gelling temperature), making more functional groups exposed and more aggregations and firmer gel networks produced. Furthermore, KGM could protect molecular interaction forces from being destroyed during further heating procedure. Consequently, the molecular interactivities like hydrogen bonding, hydrophobic interactions, and disulfide bridge within the network were enhanced (da Silva et al., 2016; Zhang, Xue, et al., 2015), making the gel more compact and strengthened. Besides, KGM would protect crystalline structures from being melted at high temperatures (Liu et al., 2021), helping enhance the gel strength and mechanical properties of the formed gel. In the earlier research (Ran, Yang, et al., 2022), we suggested that the KGM addition of 6.5% in the plant-based fishball analog could help mimic the textural characteristics and rheological performance of conventional fishball, while excessive KGM addition ($\geq$ 8.0%) could result in an exceedingly tight and rigid texture. This effect could be associated with the relatively high crystallinity index, which is related to the stiffness and rigidness of materials (McKeen, 2012).

Overall, as KGM concentration increased, the denaturation and gelling processes slowed down, contributing to molecular interactions and better aggregations and crystalline structures within the network. The significantly increased gel strength S_g (from 82.5 to 5537.6 Pa·S^n) while decreased overall tan δ (from 0.37 to 0.14) indicated the complex gel was impressively strengthened by KGM incorporation. However, too much KGM ($\geq$ 8.0%) may lead to an overly rigid and stiff gel.

3.7. Validation

3.7.1. FTIR

The conformational changes and chemical bond stretching in the structures of the SPI-KGM complex were researched through FTIR to validate the presumable schematic diagram. As shown in Fig. 8A, the spectra for samples with different KGM concentrations were nearly identical, revealing that no additional functional groups resulted from the KGM incorporation. A broad and intense absorption peak around 3200 - 3600 cm^{-1} was identified in all samples. This broad peak has been reported to signify the O–H stretching vibration and N–H stretching vibration with hydrogen-bonded, implying the presence of hydrogen bonding between polysaccharides and protein molecules (Yang, Wang, Li-Sha, & Chen, 2021). Another weak peak was identified around 2950 cm^{-1}, relevant to C–H stretching and bending vibration (Monsoor, Kalapathy, & Proctor, 2001). With augmenting KGM levels, the peak

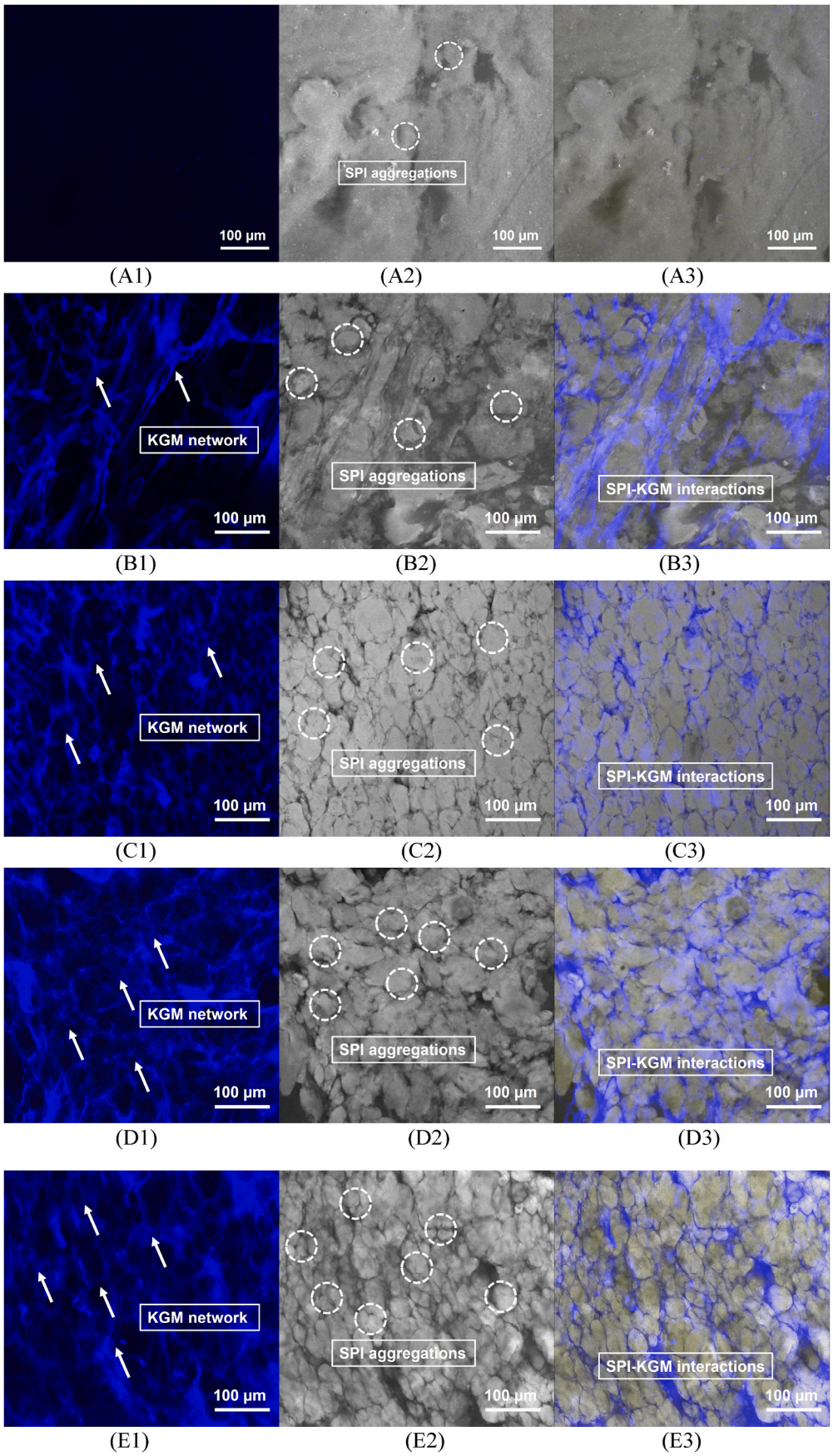

Fig. 6. (A–E) The CLSM pictures of the soy protein and konjac glucomannan complex gel with different konjac glucomannan (KGM) concentrations (0–8.0%). (A1 - E1) Calcofluor white-stained KGM, (A2 - E2) Rhodamine B-stained protein (grayscale), (A3 - E3) the overlap image for protein and KGM.

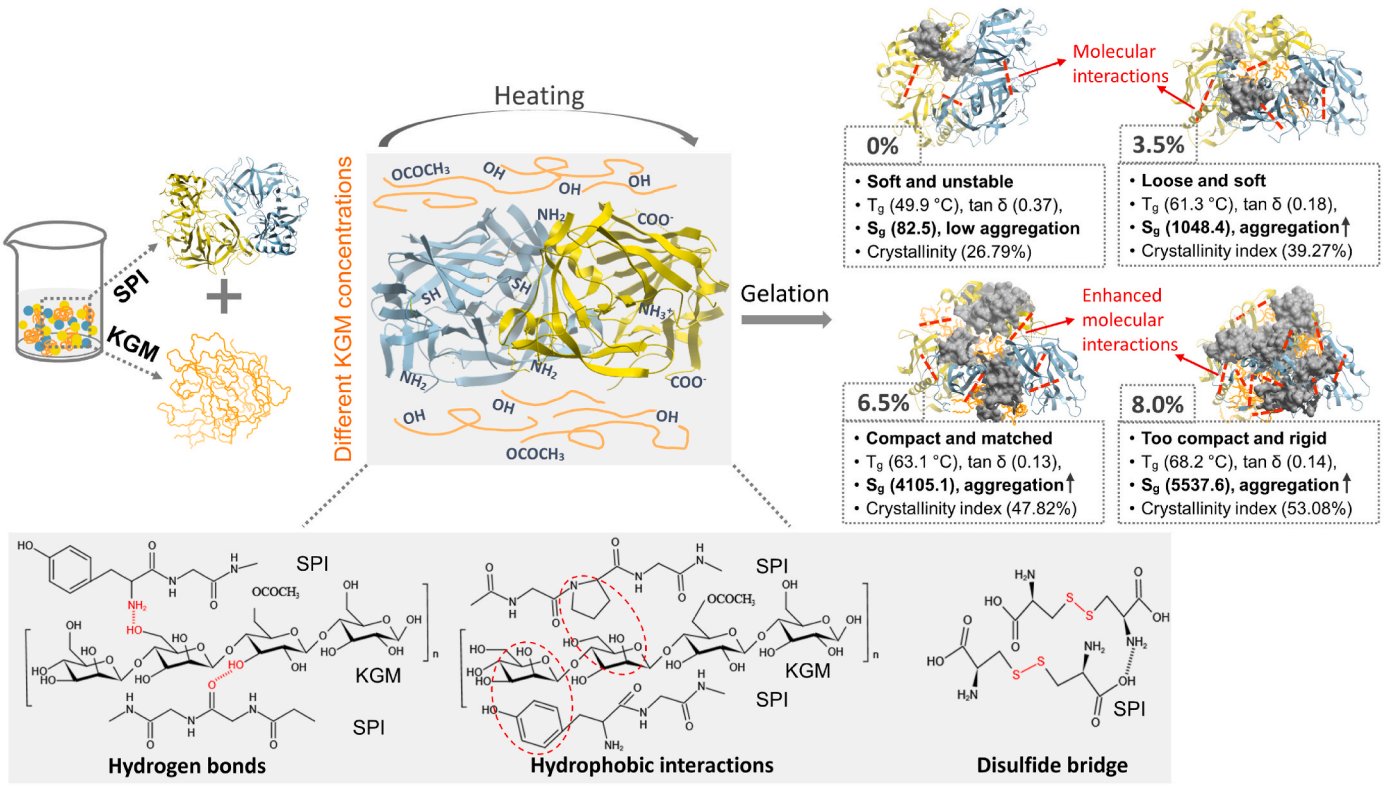

Fig. 7. A proposed schematic model for soy protein isolate (SPI)- konjac glucomannan (KGM) complex.

around the 3200 - 3600 cm^{-1} and 2950 cm^{-1} moved towards lower wavelengths, suggesting an enhancement of hydrogen bonds because of KGM incorporation. Consistently, prior research has reported that increasing the KGM concentration would promote hydrogen bonding, thus increasing the structural strength of a blend film containing deacetylated KGM (Li et al., 2018).

In addition, three peaks were observed around 1600 - 1700 cm^{-1}, 1500 - 1600 cm^{-1}, and 1230 cm^{-1}, which are related to the amide I, amide II, and amide III, respectively, resulting from C = O stretching, CN stretching/in-plane NH bending, and the CN stretching/NH bending (Min, Ma, Kuang, Huang, & Xiong, 2022, p. 107482). As shown in Fig. 8A, after KGM incorporation, the characteristics of amide II and III remained unchanged, while the amide I band tended to shift towards a lower wavelength, suggesting that the conformational state of the SPI-KGM complex with KGM tended to possess a more regulated structure. This phenomenon may confirm the increase of crystalline structures, making the gel network more regulated and ordered. Briefly, increasing KGM concentration in the SPI-KGM complex improved the conformational state and intermolecular interactions, facilitating the gel strength and viscoelastic performance of the complex gel.

3.7.2. Molecular interaction forces

Based on the solubilized protein content under the treatment of various chemical solutions, the levels of different molecular interaction forces could be indirectly inferred. As displayed in Fig. 8B, the hydrophobic interactions were the most pronounced molecular interaction force in all samples, followed by hydrogen bonds and disulfide bonds. Furthermore, as the KGM concentration in SPI-KGM increased, these molecular forces were accordingly enhanced, favoring the structure strength and stability of gel networks.

Numerous research has indicated that the physicochemical performance and structural strength of final gels depend primarily on the rate and numbers of protein denaturation and aggregation (Liu, Zhao, Xie, & Xiong, 2011; Zhang et al., 2016). During the heat-induced gelling process, proteins experience denaturation, exposing buried functional groups such as hydrophobic residues, which help the subsequent aggregation and the constitution of well-constructed three-dimensional networks. As discussed before, KGM could slow down the denaturation procedure, making more functional groups of SPI exposed, enhancing molecular interaction forces between SPI chains and between SPI and KGM molecules. Prior research suggested that the primary molecular force in soy protein gel induced by heating was hydrophobic interactions and hydrogen bridges (Sheard, Fellows, Ledward, & Mitchell, 1986). The phenomenon could be because the removal of acetyl groups during deacetylation could improve the hydrophobicity of deacetylated KGM (Xu et al., 2022), contributing to hydrophobic interactions between KGM and proteins and between KGM molecules. Besides, decreasing the moisture content in a protein system would make disulfide bonding pronounced gradually (Sheard et al., 1986). Therefore, it could be assumed that the increase of disulfide bonding in the SPI-KGM complex with increasing KGM concentration resulted from the substantial water-absorbing ability of KGM. The water molecules in the KGM-SPI system were progressively changed from free water to bound water and redistributed, leading to a stabler and more compact gel network (Li, Qu, Feng, & Chen, 2020). Consistently, Li et al. (2020) demonstrated that the presence of KGM (5%) could enhance disulfide bonding of KGM-gluten composite gel by 2.57-fold, which contributed to the stability of the gel network.

4. Conclusions

The SPI-KGM complex as a model system to further comprehend the molecular interactivities between proteins and polysaccharides in a plant-based fishball analog. KGM tremendously impacted the dynamic mechanical thermal behavior, gel strength, strain hardening, crystallinity, and microstructure of the SPI-KGM complex. Increasing KGM levels promoted the strain-hardening and gel strength, revealing more excluded volume interactions and large junction zones within complex gels. KGM could extend the duration of protein denaturation, promoted protein aggregations, enhanced gelling temperatures, and improved

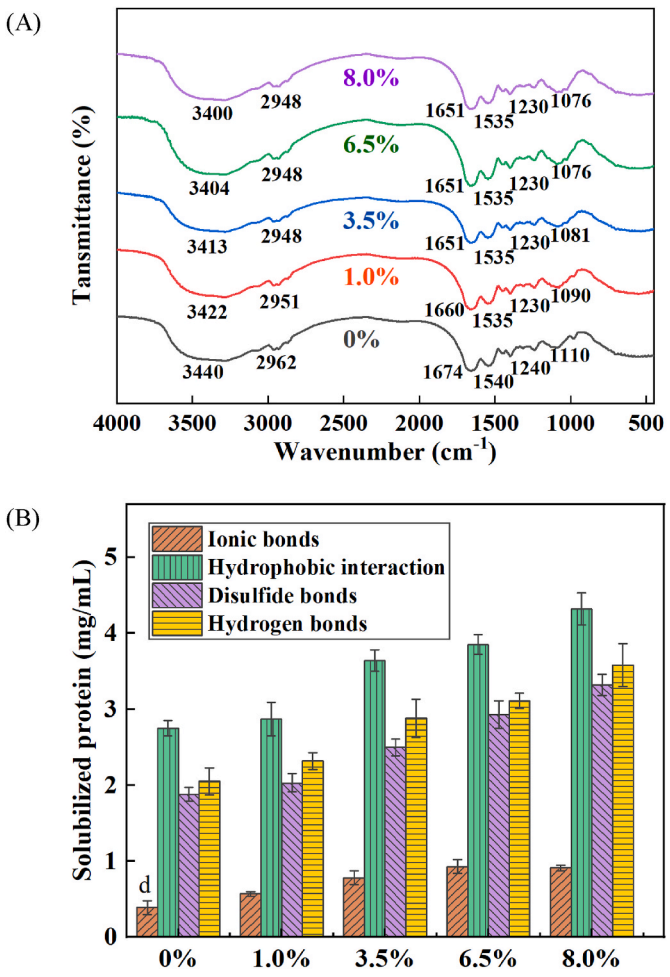

Fig. 8. (A) The FTIR spectra of soy protein (SPI)-konjac glucomannan (KGM) complex with different KGM concentrations. (B) The molecular forces (presented as solubilized protein) of the SPI-KGM complex with different KGM concentrations.

molecular interactivities. The relative crystallinity index of the SPI-KGM complex was significantly augmented with increasing KGM levels. A compact and regulated gel network was formed in the SPI-KGM complex (6.5%), while an overly tight and packed structures were formed in the complex with excessive KGM incorporation (≥8.0%). The proposed schematic model indicated that KGM addition enhanced the aggregation, molecular interactivities, and crystallinity of the KGM-SPI model system. These results help better comprehend the molecular interactions, rheological behavior, mechanical properties of plant-based fishball analogs through a KGM-SPI model system. One potential limitation in this study is that the deacetylation degree of KGM varies with increasing KGM concentration. Both KGM concentration and the degree of KGM deacetylation could affect the rheological properties. The current study mainly focusses on the influence of KGM concentration on the SPI-KGM system. Further study can investigate the influence of different deacetylation degrees on the system by changing Na_2CO_3 addition while fixing the KGM concentration in the SPI-KGM system.

Declaration of competing interest

The authors declare that they have no known competing financial interests or personal relationships that could have appeared to influence the work reported in this paper.

Data availability

The data that has been used is confidential.

Acknowledgment

The current study was finically supported by the Singapore Ministry of Education Academic Research Fund Tier 1 (R-160-000-A40-114), Applied Basic Research Project (Agricultural) Suzhou Science and Technology Planning Program (SNG2020061), and industrial support from Changzhou Wangxianglou Food Co., Ltd (R-160-000-B22-597).

Appendix A. Supplementary data

Supplementary data to this article can be found online at https://doi.org/10.1016/j.foodhyd.2022.107959.

References

Abbastabar, B., Azizi, M. H., Adnani, A., & Abbasi, S. (2015). Determining and modeling rheological characteristics of quince seed gum. *Food Hydrocolloids, 43*, 259–264.
Andoyo, R., Dianti Lestari, V., Mardawati, E., & Nurhadi, B. (2018). Fractal dimension analysis of texture formation of whey protein-based foods. *International Journal of Food Science, 2018*, Article 7673259.
Baeza, R., Carp, D., Pérez, O., & Pilosof, A. (2002). κ-Carrageenan–protein interactions: Effect of proteins on polysaccharide gelling and textural properties. *LWT–Food Science and Technology, 35*(8), 741–747.
Balani, K., Verma, V., Agarwal, A., & Narayan, R. (2014). Physical, thermal, and mechanical properties of polymers. In *Biosurfaces* (pp. 329–344).
Berghout, J., Boom, R., & Van der Goot, A. (2015). Understanding the differences in gelling properties between lupin protein isolate and soy protein isolate. *Food Hydrocolloids, 43*, 465–472.
Bernal, V., Smajda, C., Smith, J., & Stanley, D. (1987). Interactions in protein/polysaccharide/calcium gels. *Journal of Food Science, 52*(5), 1121–1125.
Bossard, F., Moan, M., & Aubry, T. (2007). Linear and nonlinear viscoelastic behavior of very concentrated plate-like kaolin suspensions. *Journal of Rheology, 51*(6), 1253–1270.
Brindley, G. W. (1980). Order–disorder in clay mineral structures. *Crystal Structures of Clay Minerals and their X-Ray Identification, 5*, 125–196.
Campbell, L. J., Gu, X., Dewar, S. J., & Euston, S. R. (2009). Effects of heat treatment and glucono-δ-lactone-induced acidification on characteristics of soy protein isolate. *Food Hydrocolloids, 23*(2), 344–351.
Cao, C., Feng, Y., Kong, B., Xia, X., Liu, M., Chen, J., et al. (2021). Textural and gel properties of frankfurters as influenced by various κ-carrageenan incorporation methods. *Meat Science, 176*, Article 108483.
Champenois, Y., Rao, M., & Walker, L. P. (1998). Influence of gluten on the viscoelastic properties of starch pastes and gels. *Journal of the Science of Food and Agriculture, 78*(1), 119–126.
Chemeda, Y. C., Deneele, D., Christidis, G. E., & Ouvrard, G. (2015). Influence of hydrated lime on the surface properties and interaction of kaolinite particles. *Applied Clay Science, 107*, 1–13.
Chen, J., Li, J., & Li, B. (2011). Identification of molecular driving forces involved in the gelation of konjac glucomannan: Effect of degree of deacetylation on hydrophobic association. *Carbohydrate Polymers, 86*(2), 865–871.
Comfort, S., & Howell, N. K. (2002). Gelation properties of soya and whey protein isolate mixtures. *Food Hydrocolloids, 16*(6), 661–672.
Dai, S., Jiang, F., Corke, H., & Shah, N. P. (2018). Physicochemical and textural properties of mozzarella cheese made with konjac glucomannan as a fat replacer. *Food Research International, 107*, 691–699.
Dekkers, B. L., Boom, R. M., & van der Goot, A. J. (2018). Structuring processes for meat analogues. *Trends in Food Science & Technology, 81*, 25–36.
Feng, T., Wang, X., Wang, X., Xia, S., & Huang, Q. (2021). Plant protein-based antioxidant Pickering emulsions and high internal phase Pickering emulsions against broad pH range and high ionic strength: Effects of interfacial rheology and microstructure. *LWT–Food Science and Technology, 150*, Article 111953.
Galante, M., Boeris, V., Álvarez, E., & Risso, P. (2017). Microstructural and textural properties of rennet-induced milk protein gel: Effect of guar gum. *International Journal of Food Properties, 20*(sup3), S2569–S2578.
Geremias-Andrade, I. M., Souki, N. P., Moraes, I. C., & Pinho, S. C. (2017). Rheological and mechanical characterization of curcumin-loaded emulsion-filled gels produced with whey protein isolate and xanthan gum. *LWT–Food Science and Technology, 86*, 166–173.
Han, Z., Xu, S., Sun, J., Yue, X., Wu, Z., & Shao, J. H. (2021). Effects of fatty acid saturation degree on salt-soluble pork protein conformation and interfacial adsorption characteristics at the oil/water interface. *Food Hydrocolloids, 113*, Article 106472.
He, S., Gu, C., Wang, D., Xu, W., Wang, R., & Ma, Y. (2020). The stability and *in vitro* digestion of curcumin emulsions containing konjac glucomannan. *LWT–Food Science and Technology, 117*, Article 108672.

Hermansson, A.-M. (1986). Soy protein gelation. *Journal of the American Oil Chemists Society, 63*(5), 658–666.
Herranz, B., Tovar, C. A., Solo-de-Zaldívar, B., & Borderias, A. J. (2012). Effect of alkalis on konjac glucomannan gels for use as potential gelling agents in restructured seafood products. *Food Hydrocolloids, 27*(1), 145–153.
Hesarinejad, M. A., Koocheki, A., & Razavi, S. M. A. (2014). Dynamic rheological properties of *Lepidium perfoliatum* seed gum: Effect of concentration, temperature and heating/cooling rate. *Food Hydrocolloids, 35*, 583–589.
Hogan, S. A., Daly, D. F., & McCarthy, N. A. (2021). Rheological and solubility properties of soy protein isolate. *Molecules, 26*(10), 3015.
Huang, M., Mao, Y., Li, H., & Yang, H. (2021). Kappa-carrageenan enhances the gelation and structural changes of egg yolk via electrostatic interactions with yolk protein. *Food Chemistry, 360*, Article 129972.
Huang, M., Mao, Y., Mao, Y., & Yang, H. (2022). Xylitol and maltitol improve the rheological property of kappa-carrageenan. *Foods, 11*(1), 51.
Huang, M., Theng, A. H. P., Yang, D., & Yang, H. (2021). Influence of κ-carrageenan on the rheological behaviour of a model cake flour system. *LWT–Food Science and Technology, 136*, Article 110324.
Hu, Y., Tian, J., Zou, J., Yuan, X., Li, J., Liang, H., et al. (2019). Partial removal of acetyl groups in konjac glucomannan significantly improved the rheological properties and texture of konjac glucomannan and κ-carrageenan blends. *International Journal of Biological Macromolecules, 123*, 1165–1171.
Iglesias-Otero, M. A., Borderías, J., & Tovar, C. A. (2010). Use of konjac glucomannan as additive to reinforce the gels from low-quality squid surimi. *Journal of Food Engineering, 101*(3), 281–288.
Jiang, S., Ma, Y., Wang, Y., Wang, R., & Zeng, M. (2022). Effect of κ-carrageenan on the gelation properties of oyster protein. *Food Chemistry, 382*, Article 132329.
Kumar, L., Brennan, M., Brennan, C., & Zheng, H. (2022). Thermal, pasting and structural studies of oat starch-caseinate interactions. *Food Chemistry, 373*, Article 131433.
Lei, Y.-c., Zhao, X., Li, D., Wang, L.-j., & Wang, Y. (2022). Effects of κ-Carrageenan and guar gum on the rheological properties and microstructure of phycocyanin gel. *Foods, 11*(5), 734.
Liang, W.-L., Liao, J.-S., Qi, J.-R., Jiang, W.-X., & Yang, X.-Q. (2022). Physicochemical characteristics and functional properties of high methoxyl pectin with different degree of esterification. *Food Chemistry, 375*, Article 131806.
Li, J., Ma, J., Chen, S., He, J., & Huang, Y. (2018). Characterization of calcium alginate/deacetylated konjac glucomannan blend films prepared by Ca^{2+} crosslinking and deacetylation. *Food Hydrocolloids, 82*, 363–369.
Li, S., Qu, Z., Feng, J., & Chen, Y. (2020). Improved physicochemical and structural properties of wheat gluten with konjac glucomannan. *Journal of Cereal Science, 95*, Article 103050.
Liu, S., Bao, H., & Li, L. (2016). Thermoreversible gelation and scaling laws for graphene oxide-filled κ-carrageenan hydrogels. *European Polymer Journal, 79*, 150–162.
Liu, Y., Chen, Q., Fang, F., Liu, J., Wang, Z., Chen, H., et al. (2021). The influence of Konjac glucomannan on the physicochemical and rheological properties and microstructure of canna starch. *Foods, 10*(2), 422.
Liu, K. S., & Hsieh, F.-H. (2007). Protein–protein interactions in high moisture-extruded meat analogs and heat-induced soy protein gels. *Journal of the American Oil Chemists' Society, 84*(8), 741–748.
Liu, R., Zhao, S.-M., Xie, B.-J., & Xiong, S.-B. (2011). Contribution of protein conformation and intermolecular bonds to fish and pork gelation properties. *Food Hydrocolloids, 25*(5), 898–906.
Li, Z., Wang, J., Zheng, B., & Guo, Z. (2019). Effects of high pressure processing on gelation properties and molecular forces of myosin containing deacetylated konjac glucomannan. *Food Chemistry, 291*, 117–125.
Lu, L., Liu, X., & Tong, Z. (2006). Critical exponents for sol–gel transition in aqueous alginate solutions induced by cupric cations. *Carbohydrate Polymers, 65*(4), 544–551.
Luo, X., He, P., & Lin, X. (2013). The mechanism of sodium hydroxide solution promoting the gelation of konjac glucomannan (KGM). *Food Hydrocolloids, 30*(1), 92–99.
Maruyama, N., Adachi, M., Takahashi, K., Yagasaki, K., Kohno, M., Takenaka, Y., et al. (2001). Crystal structures of recombinant and native soybean β-conglycinin β homotrimers. *European Journal of Biochemistry, 268*(12), 3595–3604.
Matos, M. E., Sanz, T., & Rosell, C. M. (2014). Establishing the function of proteins on the rheological and quality properties of rice based gluten free muffins. *Food Hydrocolloids, 35*, 150–158.
McKeen, L. (2012). Introduction to the physical, mechanical, and thermal properties of plastics and elastomers. In *The effect of sterilization methods on plastics and elastomers* (pp. 57–84). Amsterdam, The Netherlands: Elsevier.
Min, C., Ma, W., Kuang, J., Huang, J., & Xiong, Y. L. (2022). *Textural properties, microstructure and digestibility of mungbean starch–flaxseed protein composite gels*. Food Hydrocolloids.
Monsoor, M., Kalapathy, U., & Proctor, A. (2001). Determination of polygalacturonic acid content in pectin extracts by diffuse reflectance Fourier transform infrared spectroscopy. *Food Chemistry, 74*(2), 233–238.
Niu, L., Zhou, X., Yuan, C., Bai, Y., Lai, K., Yang, F., et al. (2013). Characterization of tilapia (Oreochromis niloticus) skin gelatin extracted with alkaline and different acid pretreatments. *Food Hydrocolloids, 33*(2), 336–341.
Rafe, A., & Razavi, S. M. (2013). Dynamic viscoelastic study on the gelation of basil seed gum. *International Journal of Food Science and Technology, 48*(3), 556–563.
Ran, X., Lou, X., Zheng, H., Gu, Q., & Yang, H. (2022). Improving the texture and rheological qualities of a plant-based fishball analogue by using konjac glucomannan to enhance crosslinks with soy protein. *Innovative Food Science & Emerging Technologies, 75*, Article 102910.
Ran, X., Yang, Z., Chen, Y., & Yang, H. (2022). Konjac glucomannan decreases metabolite release of a plant-based fishball analogue during in vitro digestion by affecting amino acid and carbohydrate metabolic pathways. *Food Hydrocolloids, 129*, Article 107623.
Renkema, J. M., & van Vliet, T. (2002). Heat-induced gel formation by soy proteins at neutral pH. *Journal of Agricultural and Food Chemistry, 50*(6), 1569–1573.
Rønholt, S., Kirkensgaard, J. J. K., Pedersen, T. B., Mortensen, K., & Knudsen, J. C. (2012). Polymorphism, microstructure and rheology of butter. Effects of cream heat treatment. *Food Chemistry, 135*(3), 1730–1739.
Sha, L., & Xiong, Y. L. (2020). Plant protein-based alternatives of reconstructed meat: Science, technology, and challenges. *Trends in Food Science & Technology, 102*, 51–61.
Sheard, P., Fellows, A., Ledward, D., & Mitchell, J. (1986). Macromolecular changes associated with the heat treatment of soya isolate. *International Journal of Food Science and Technology, 21*(1), 55–60.
da Silva, D. F., de Souza Ferreira, S. B., Bruschi, M. L., Britten, M., & Matumoto-Pintro, P. T. (2016). Effect of commercial konjac glucomannan and konjac flours on textural, rheological and microstructural properties of low fat processed cheese. *Food Hydrocolloids, 60*, 308–316.
Solo-de-Zaldívar, B., Tovar, C., Borderías, A., & Herranz, B. (2014). Effect of deacetylation on the glucomannan gelation process for making restructured seafood products. *Food Hydrocolloids, 35*, 59–68.
Sow, L. C., Nicole Chong, J. M., Liao, Q. X., & Yang, H. (2018). Effects of κ-carrageenan on the structure and rheological properties of fish gelatin. *Journal of Food Engineering, 239*, 92–103.
Sow, L. C., Tan, S. J., & Yang, H. (2019). Rheological properties and structure modification in liquid and gel of tilapia skin gelatin by the addition of low acyl gellan. *Food Hydrocolloids, 90*, 9–18.
Sow, L. C., Toh, N. Z. Y., Wong, C. W., & Yang, H. (2019). Combination of sodium alginate with tilapia fish gelatin for improved texture properties and nanostructure modification. *Food Hydrocolloids, 94*, 459–467.
Speroni, F., Beaumal, V., de Lamballerie, M., Anton, M., Añón, M. C., & Puppo, M. C. (2009). Gelation of soybean proteins induced by sequential high-pressure and thermal treatments. *Food Hydrocolloids, 23*(5), 1433–1442.
Su, J.-F., Huang, Z., Yuan, X.-Y., Wang, X.-Y., & Li, M. (2010). Structure and properties of carboxymethyl cellulose/soy protein isolate blend edible films crosslinked by Maillard reactions. *Carbohydrate Polymers, 79*(1), 145–153.
Tatirat, O., & Charoenrein, S. (2011). Physicochemical properties of konjac glucomannan extracted from konjac flour by a simple centrifugation process. *LWT–Food Science and Technology, 44*(10), 2059–2063.
Totosaus, A., Montejano, J. G., Salazar, J. A., & Guerrero, I. (2002). A review of physical and chemical protein-gel induction. *International Journal of Food Science and Technology, 37*(6), 589–601.
Wang, Y., Chen, Y., Zhou, Y., Nirasawa, S., Tatsumi, E., Li, X., et al. (2017). Effects of konjac glucomannan on heat-induced changes of wheat gluten structure. *Food Chemistry, 229*, 409–416.
Wang, C.-S., Virgilio, N., Wood-Adams, P. M., & Heuzey, M.-C. (2018). A gelation mechanism for gelatin/polysaccharide aqueous mixtures. *Food Hydrocolloids, 79*, 462–472.
Wang, S., Zhou, B., Wang, Y., & Li, B. (2015). Preparation and characterization of konjac glucomannan microcrystals through acid hydrolysis. *Food Research International, 67*, 111–116.
Wu, C., Hua, Y., Chen, Y., Kong, X., & Zhang, C. (2017). Effect of temperature, ionic strength and 11S ratio on the rheological properties of heat-induced soy protein gels in relation to network proteins content and aggregates size. *Food Hydrocolloids, 66*, 389–395.
Xiong, G., Cheng, W., Ye, L., Du, X., Zhou, M., Lin, R., et al. (2009). Effects of konjac glucomannan on physicochemical properties of myofibrillar protein and surimi gels from grass carp (*Ctenopharyngodon idella*). *Food Chemistry, 116*(2), 413–418.
Xu, L., Wang, J., Lv, Y., Su, Y., Chang, C., Gu, L., et al. (2022). Influence of konjac glucomannan on the emulsion-filled/non-filled chicken gel: Study on intermolecular forces, microstructure and gelling properties. *Food Hydrocolloids, 124*, Article 107269.
Yang, Q., Wang, Y.-R., Li-Sha, Y.-J., & Chen, H.-Q. (2021). The effects of basil seed gum on the physicochemical and structural properties of arachin gel. *Food Hydrocolloids, 110*, Article 106189.
Yang, Z., Yang, H., & Yang, H. (2018). Effects of sucrose addition on the rheology and microstructure of κ-carrageenan gel. *Food Hydrocolloids, 75*, 164–173.
Yuan, C., Xu, D., Cui, B., & Wang, Y. (2019). Gelation of κ-carrageenan/konjac glucommanan compound gel: Effect of cyclodextrins. *Food Hydrocolloids, 87*, 158–164.
Yuan, L., Yu, J., Mu, J., Shi, T., Sun, Q., Jin, W., et al. (2019). Effects of deacetylation of konjac glucomannan on the physico-chemical properties of surimi gels from silver carp (*Hypophthalmichthys molitrix*). *RSC Advances, 9*(34), 19828–19836.
Zhang, T., Li, Z., Wang, Y., Xue, Y., & Xue, C. (2016). Effects of konjac glucomannan on heat-induced changes of physicochemical and structural properties of surimi gels. *Food Research International, 83*, 152–161.
Zhang, Q.-T., Tu, Z.-C., Wang, H., Huang, X.-Q., Fan, L.-L., Bao, Z.-Y., et al. (2015). Functional properties and structure changes of soybean protein isolate after subcritical water treatment. *Journal of Food Science & Technology, 52*(6), 3412–3421.
Zhang, T., Xue, Y., Li, Z., Wang, Y., & Xue, C. (2015). Effects of deacetylation of konjac glucomannan on *Alaska Pollock* surimi gels subjected to high-temperature (120 °C) treatment. *Food Hydrocolloids, 43*, 125–131.
Zhang, H., Yang, L., Tu, Y., Wu, N., Jiang, Y., & Xu, M. (2019). Changes in texture and molecular forces of heated-induced egg white gel with adding xanthan gum. *Journal of Food Process Engineering, 42*(4), Article e13071.

Zhao, H., Chen, J., Hemar, Y., & Cui, B. (2020). Improvement of the rheological and textural properties of calcium sulfate-induced soy protein isolate gels by the incorporation of different polysaccharides. *Food Chemistry, 310*, Article 125983.

Zhou, Y., Cao, H., Hou, M., Nirasawa, S., Tatsumi, E., Foster, T. J., et al. (2013). Effect of konjac glucomannan on physical and sensory properties of noodles made from low-protein wheat flour. *Food Research International, 51*(2), 879–885.

Zhou, Y., Winkworth-Smith, C. G., Wang, Y., Liang, J., Foster, T. J., & Cheng, Y. (2014). Effect of a small amount of sodium carbonate on konjac glucomannan-induced changes in thermal behavior of wheat starch. *Carbohydrate Polymers, 114*, 357–364.

Zhuang, X., Wang, L., Jiang, X., Chen, Y., & Zhou, G. (2021). Insight into the mechanism of myofibrillar protein gel influenced by konjac glucomannan: Moisture stability and phase separation behavior. *Food Chemistry, 339*, Article 127941.